

Magnetic Axial Dependency of $H\alpha$ Emission Location in Peripheral Plasmas of Large Helical Device as Determined by Plasma Polarization Spectroscopy

Atsushi IWAMAE^{a)}, Atsushi SAKAUE, Nobuhiro NESHI,
Jun YANAGIBAYASHI, Masahiro HASUO, Daisuke NAKAMURA¹⁾, Keiji SAWADA¹⁾,
Motoshi GOTO²⁾ and Shigeru MORITA²⁾

Department of Mechanical Engineering and Science Kyoto University, Kyoto 606-8501, Japan

¹⁾*Faculty of Engineering, Shinshu University, Wakasato, Nagano 380-8553, Japan*

²⁾*National Institute for Fusion Science, Toki, Gifu 509-5292, Japan*

(Received 28 April 2010 / Accepted 14 July 2010)

The behavior of hydrogen neutral particles in and around the ergodic layer of Large Helical Device plasmas has been investigated through $H\alpha$ emission spectral line profiles using plasma polarization spectroscopy (PPS). The PPS technique enables us to quantitatively evaluate emission locations, atomic temperatures and velocity components along the line-of-sight (LOS) for both inner and outer peripheral regions. The emission locations and the LOS components of atomic velocities are determined by varying the magnetic field axis R_{ax} from 3.60 m to 4.00 m, shot by shot. The high intensity region of $H\alpha$ emissions is localized in the inner ergodic layer for the inward configuration. With an increase in R_{ax} , the high intensity region of $H\alpha$ emission moves outward.

© 2010 The Japan Society of Plasma Science and Nuclear Fusion Research

Keywords: hydrogen Balmer α , polarization, neutral particle transport, spectral line profile, peripheral plasma

DOI: 10.1585/pfr.5.032

1. Introduction

For next-generation nuclear fusion reactors such as ITER [1], hydrogen recycling from the peripheral plasma is one of the key issues responsible for controlling fueling into and pumping from magnetically confined fusion plasmas. The edge, scrape-off-layer (SOL) and divertor area of the plasmas are known to significantly influence core plasma confinement and vice versa [2]. As a result, the knowledge of atomic and molecular processes in the SOL and divertor regions has become more important.

In order to measure tritium recycling in the Tokamak Fusion Test Reactor (TFTR) plasma, $T\alpha$, $D\alpha$ and $H\alpha$ were monitored at a high wavelength resolution using a Fabry-Perot interferometer [3, 4]. In order to observe the inboard toroidal limiter, a polarization filter was placed in front of the telescope lens and oriented to transmit only the unshifted π component. Regarding dissociation products in the 10 eV \sim 100 eV atomic temperature range, there were some inconsistencies between the observed and simulated spectra as calculated using the neutral Monte-Carlo code DEGAS [3].

Spectral profiles of the $D\alpha$ line from the divertor region of the JT-60U have been observed with a high-resolution spectrometer and analyzed through simulations using a three-dimensional neutral particle transport

code [5, 6]. Narrow and broad components make up the spectral profile. The profiles indicate that the narrow component arises as a result of dissociative excitation and electron collisional excitation of atoms produced by dissociation, while the broad component is attributed to the electron collisional excitation of atoms produced by reflection and charge exchange.

The spectral profiles of He I have been observed for Large Helical Device (LHD) plasmas using a high resolution spectrometer [7]. Through the Zeeman splitting of the He I spectra, the location of the emissions has been well identified on a map of the poloidal cross section as being just outside the region of the ergodic layer where the magnetic field line structure is chaotic (Fig. 1 in Ref. [7]). On the other hand for the $H\alpha$ emission from the LHD plasma, it is difficult to apply the same technique to identify the emission location because of the broadening of the spectral line profile. The plasma polarization spectroscopy (PPS) technique [8] is applied to identify the $H\alpha$ emission, since the magnetic field directions are different for the inner and outer poloidal LHD plasma. The π and σ Zeeman polarization components provide additional information to identify the emission location of the hydrogen atoms, their temperatures and the line-of-sight (LOS) components of atomic velocities. The polarization separated $H\alpha$ profiles are interpreted as superpositions of Zeeman profiles at the two locations of the different magnetic field strengths near the equatorial plane (Ref. [9] and references therein). The be-

author's e-mail: iwamae.atsushi@jaea.go.jp

^{a)} present address: Fusion Research and Development Directorate, Japan Atomic Energy Agency, Naka, Ibaraki 311-0193, Japan

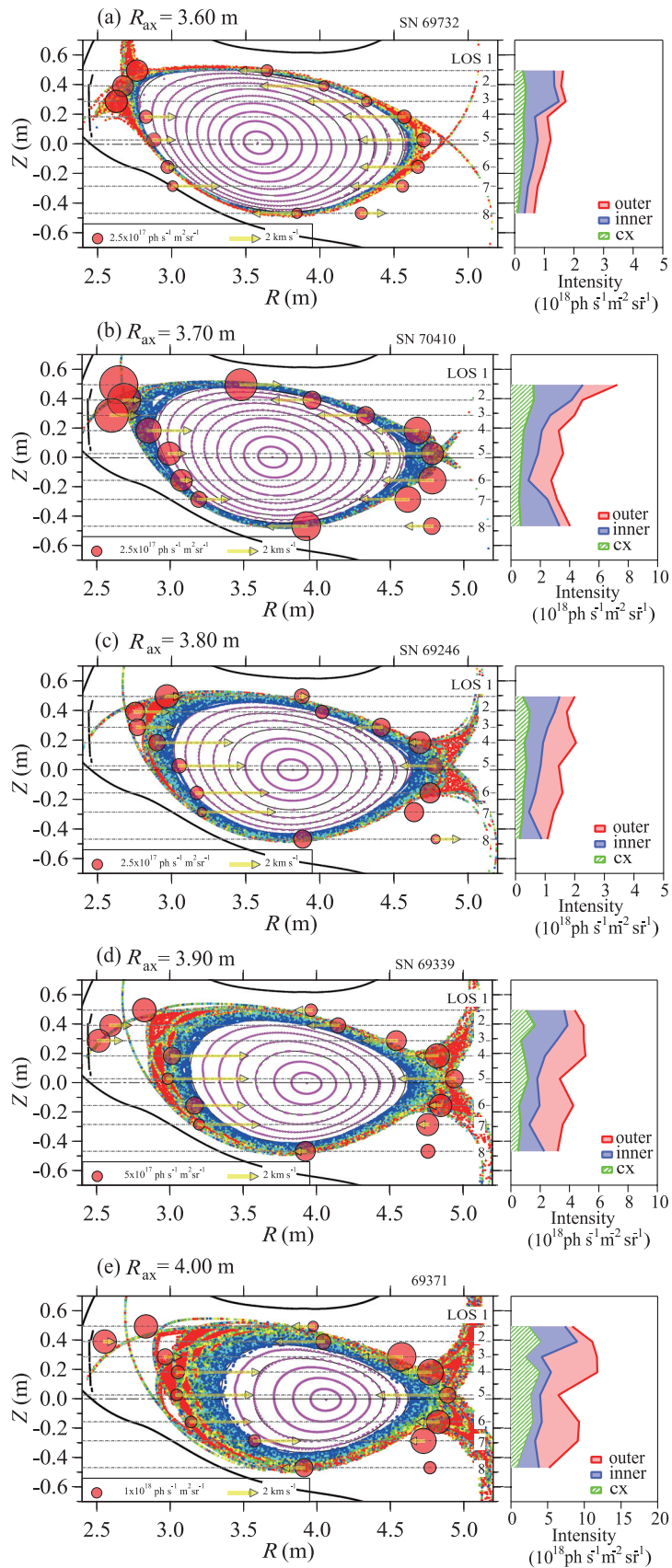


Fig. 1 Ergodic layers, experimentally determined Ha emission locations, and intensities for different magnetic axial configurations: (a) $R_{ax} = 3.60 \text{ m}$, (b) $R_{ax} = 3.70 \text{ m}$, (c) $R_{ax} = 3.80 \text{ m}$, (d) $R_{ax} = 3.90 \text{ m}$, and (e) $R_{ax} = 4.00 \text{ m}$. Colors of the magnetic field lines are defined in Table 1. The sum of the inner, outer, and charge exchange intensity components are indicated in the right-hand boxes.

havior of neutral particles in the plasma periphery has been investigated by a three-dimensional neutral particle transport simulation code (EIRENE for LHD [10]), which assumes that the distribution of the plasma flow onto the divertor plates corresponds to the strike points calculated by magnetic field line traces.

In this experiment, we have increased the number of LOS equipped with polarization separation optics to cover the poloidal cross section of the plasma in order to map the emission locations at its cross section. We have analyzed the H α emissions from LHD plasmas, wherein the magnetic field axis R_{ax} has been varied from 3.6 m to 4.0 m, shot by shot.

2. Experimental Setup

LHD with the parameters $R/a = 3.6 \text{ m}/0.64 \text{ m}$, $B_t \leq 3 \text{ T}$, and $V_p = 30 \text{ m}^3$ [11], is characterized by ergodic layers, a stochastic magnetic field surrounding the core plasma. Figure 1 shows the plot of the magnetic field lines for $R_{ax} = 3.60 \text{ m}$, 3.70 m , 3.80 m , 3.90 m and 4.00 m at the observed poloidal cross section from the observation port. Table 1 indicates the corresponding colors of the length of the magnetic field lines in the ergodic layer. The thickness of the ergodic layer typically varies from 20 mm to 300 mm, primarily depending on the poloidal angle and the position of the magnetic axis which varied from 3.5 m to 4.1 m. We used the “LHD_Line_of_Force.exe” [12] computer code to plot magnetic field lines.

We observed LHD plasmas initiated by two of three electron cyclotron heating (ECH) beams of 82.7 GHz, 84 GHz and/or 168 GHz, respectively. From 0.30 s, the plasmas were mainly sustained by three neutral beam injections (NBIs). The ECH beams were stopped at 0.50 s at the latest. We measured the polarization separated H α line profiles while varying the magnetic axis R_{ax} of the NBI-heated plasmas to 3.60 m, 3.70 m, 3.80 m, 3.90 m and 4.00 m, shot by shot. Hydrogen emissions in the LHD plasma were observed from one of the spectroscopic observation ports (Fig. 3 in Ref. [9]). The eight horizontal viewing LOS cover the poloidal cross section of the plasmas as shown in Fig. 1. The cross section of the plasma is elongated in the major radius direction. The magnetic field \mathbf{B} may be determined mainly by the current flowing

through the external coils. The magnetic field strength \mathbf{B} is saddle-shaped and highest near the helical coil (Fig. 1 in Ref. [9]). The strength and direction of the magnetic field along each viewing chord is well-defined for each LOS. Table 2 shows the height Z and polarization direction angle α of each LOS. The definition of the magnetic field vector ($|B|$, θ , ϕ) and the polarization components parallel to the direction of α and perpendicular to $\alpha - 90^\circ$ is presented (Fig. 7 in Ref. [9]).

H α line emissions were resolved into two orthogonally polarized components by the polarization separation optical system. We used beam-splitting Glan-Thompson polarizers for LOS 1, 2, 4, 6 and 7, and Glan-Taylor polarizers for LOS 3, 5 and 8 (Fig. 4 in Ref. [9]). Each of the linearly polarized extraordinary (e-)rays and ordinary (o-)rays was focused by a lens onto the input of an optical fiber having a 400 μm core diameter. Each fiber was connected to another optical fiber, a few hundred meters in length, to transmit the light to the diagnostics room. The transmitted light was dispersed by an aberration-corrected Czerny-Turner spectrometer ($f = 1 \text{ m}$) equipped with a 2400 grooves/mm grating and recorded with a charge-coupled device (CCD: 1024 \times 1024 of 13 μm square pixels). The linear dispersion of the spectrometer was 0.00281 nm/pixel (0.216 nm/mm) at the wavelength $\lambda = 656.28 \text{ nm}$ in the first order. Non-appreciable emission

Table 2 Location of each line-of-sight: height Z and axial rotation angle α of polarization separation optical components.

Line-of-sight	Z (m)	α	Instrumental width (fwhm), in pixels	
			e-ray	o-ray
1	0.495	29.8°	2.06	2.00
2	0.391	30.1°	1.94	1.88
3	0.286	48.9°	1.71	1.66
4	0.182	40.6°	1.66	1.53
5	0.026	44.0°	1.60	1.59
6	-0.156	50.6°	1.55	1.47
7	-0.286	69.2°	1.52	1.52
8	-0.469	89.4°	1.64	1.67

Table 3 Plasma configurations used for H α line profile analysis. Magnetic axial position R_{ax} and magnetic field strength B_t . Negative B_t means that the magnetic field direction is counter-clock wise as viewed from the top.

R_{ax} (m)	B_t (T)	Shot No.	Exposed Time
3.60	-2.750	69732	0.7941 s – 0.9441 s
3.70	2.676	70410	0.5745 s – 0.6745 s
3.80	-2.539	69246	0.9936 s – 1.0936 s
3.90	-2.539	69339	0.6159 s – 0.7159 s
4.00	-2.475	69371	0.4647 s – 0.6147 s

Table 1 Colors of the plotted magnetic field lines.

Connection length	Plotted color
$L_{cni} \leq 12.25 \text{ m}$	not plotted
$L_{cni} \leq 24.5 \text{ m}$ (= 1 toroidal turn)	red
$L_{cni} \leq 49.0 \text{ m}$ (= 2 toroidal turns)	yellow
$L_{cni} \leq 122.5 \text{ m}$ (= 5 toroidal turns)	green
$L_{cni} \leq 245.0 \text{ m}$ (= 10 toroidal turns)	sky blue
$L_{cni} \leq 490.0 \text{ m}$ (= 20 toroidal turns)	blue
$L_{cni} \geq 490.0 \text{ m}$ (= 20 toroidal turns)	magenta

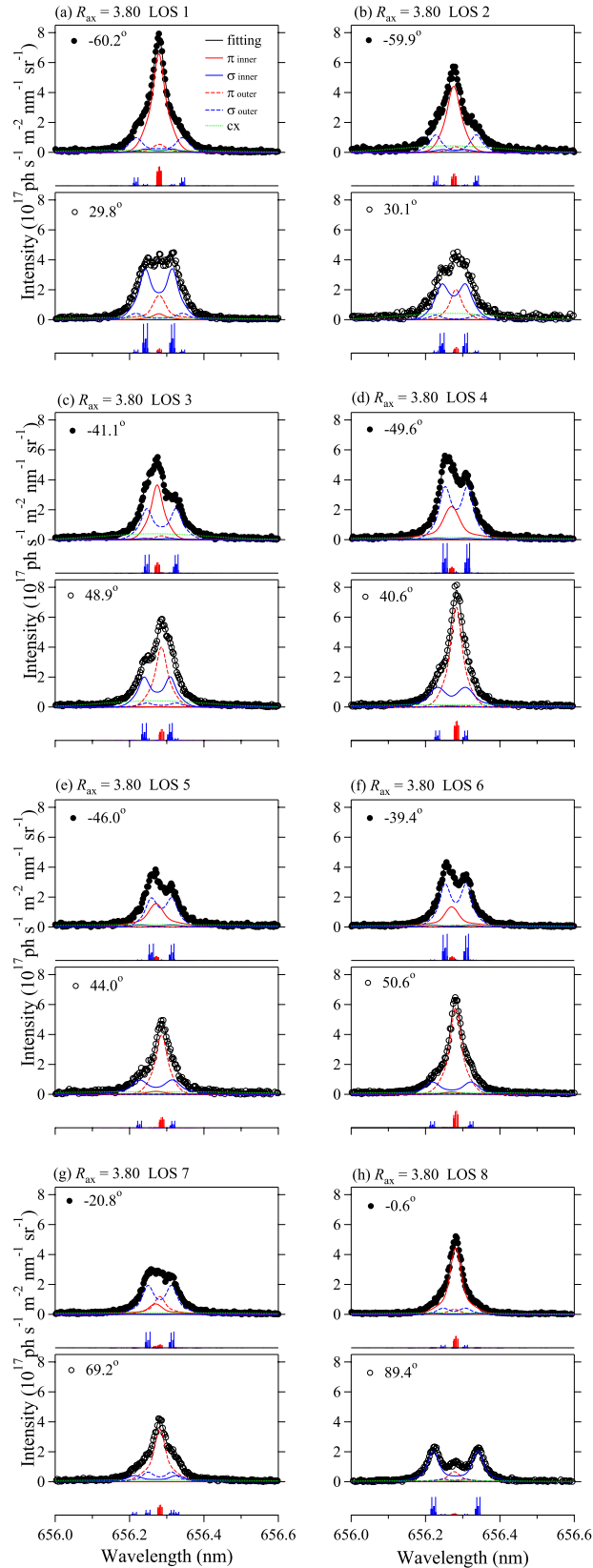


Fig. 2 Polarization-separated spectral profiles observed at: (a) LOS 1, (b) LOS 2, (c) LOS 3, (d) LOS 4, (e) LOS 5, (f) LOS 6, (g) LOS 7, and (h) LOS 8. Open and filled circles represent the observed spectra on the LOS. The polarization directions are orthogonal to each other. The least-square-fitted spectra are plotted in the solid black curves.

lines were found in the observed wavelength regions of the second and third orders. For a wavelength reference, we used a Th-Ar hollow cathode lamp [13]. The inner wall of the vacuum vessel opposite the observation port was covered by stainless steel tiles, which were sandblasted to reduce direct reflection [14].

For the observation of the plasmas of $R_{ax} = 3.60$ m and 4.00 m, the exposure and repetition times were 150 ms and 251.6 ms, respectively, for the plasmas of $R_{ax} = 3.70$ m, 3.80 m, and 3.90 m, the exposure and repetition times were 100 ms and 201.6 ms, respectively. Table 3 shows the magnetic axial position R_{ax} , the toroidal magnetic field strength B_t , the shot number for the measured shots, and the exposure times of the analyzed spectra in the shots. We chose similar conditions for the plasmas, where three NBIs were injected at a power of around 12 MW, and the plasma densities were constant at around $\bar{n}_e = 1 \times 10^{19} \text{ m}^{-3}$. The central ion temperatures ranged from 0.5 to 1.2 keV. The emission locations of $H\alpha$ are expected in the SOL and divertor plasma, where the electron temperature is less than 100 eV.

Figure 2 depicts examples of the observed spectra from LOS 1 to 8 for the plasma of $R_{ax} = 3.80$ m using filled and open circles. The upper and lower frames show the polarization-separated spectra for the linearly polarized components, with the angles $\alpha - 90^\circ$ and α , respectively. The least-square-fitted spectra are plotted in solid black curves. The π - and σ -light components from inner emission points are plotted in solid red and blue curves, while the components from the outer emission points are plotted in dashed red and blue curves, respectively. The charge exchange components have broad spectral profiles, plotted in dotted green curves. Figure 2 (a)-(h) shows that, generally speaking, the middle spectral peak of the lower frame is shifted slightly towards the longer wavelength, while the middle spectral peak of the upper frame is shifted slightly towards the shorter wavelength. These peak shifts show that atoms that emit $H\alpha$ light move from the periphery into the core plasma [9]. It can be deduced from the peak shown in the lower frame that the spectrum consists of the π dominant component of $H\alpha$ emitted by the atoms in the exterior region of emissions, which moves away from the observer, and the σ dominant component in the interior region of emissions; while in the upper frame, the spectra consists of the π dominant component emitted by the atoms in the interior region of emissions, which moves toward the observer, and the σ dominant component in the exterior region of emissions.

3. Results and Discussion

The $H\alpha$ line consists of 48 allowed and 6 ΔJ -forbidden fine-structure components (18π and 30σ allowed, 2π and 4σ ΔJ forbidden). The corresponding line strengths and line shifts of the fine structure Zeeman components were taken into account in the fitting procedure.

Table 4 Fitted results from LOS 1 to 8 for the plasma of $R_{ax} = 3.80$ m, the inner and outer H α emission locations, emission intensities, temperatures and velocity components along the LOS of cold, warm, hot atomic components.

LOS		inner		outer	
		cold	warm	cold	warm
LOS 1	hot				
R (m)	...	2.97		3.88	
B (T)	...	1.95		3.38	
θ (deg)	...	-46.2		-0.19	
ϕ (deg)	...	-6.32		20.1	
Emission intensity (10^{18} ph s $^{-1}$ m $^{-2}$ sr $^{-1}$)	0.249	1.240		0.511	
T_a (eV)	85.9	0.20	1.82	0.5	9.1
v_{LOS} (10^3 m/s)	22.8	1.00		0.52	
Relative proportion (%)	12.4	13.8	48.2	12.5	13.1
LOS 2					
R (m)	...	2.75		4.02	
B (T)	...	1.68		2.93	
θ (deg)	...	-52.7		6.71	
ϕ (deg)	...	-25.4		18.1	
Emission intensity (10^{18} ph s $^{-1}$ m $^{-2}$ sr $^{-1}$)	0.475	0.843		0.318	
T_a (eV)	39.3	0.26	1.56	0.21	1.40
v_{LOS} (10^3 m/s)	8.90	2.36		-0.45	
Relative proportion (%)	27.4	10.1	38.6	6.6	17.3
LOS 3					
R (m)	...	2.77		4.41	
B (T)	...	1.77		2.09	
θ (deg)	...	-49.6		26.1	
ϕ (deg)	...	-23.4		15.9	
Emission intensity (10^{18} ph s $^{-1}$ m $^{-2}$ sr $^{-1}$)	0.451	0.634		0.736	
T_a (eV)	84.8	0.08	0.78	0.44	6.55
v_{LOS} (10^3 m/s)	19.7	2.54		-1.87	
Relative proportion (%)	24.8	3.4	31.4	19.8	20.6
LOS 4					
R (m)	...	2.90		4.68	
B (T)	...	2.03		1.63	
θ (deg)	...	-38.4		38.8	
ϕ (deg)	...	-15.2		9.44	
Emission intensity (10^{18} ph s $^{-1}$ m $^{-2}$ sr $^{-1}$)	0.304	0.625		1.111	
T_a (eV)	151	0.76	12.9	0.24	1.76
v_{LOS} (10^3 m/s)	14.3	5.11		-0.83	
Relative proportion (%)	14.9	14.8	15.8	17.2	37.2

Section III of Ref. [9] describes the details regarding the method of analysis of the polarization-separated Zeeman H α spectra.

We assumed that there were two regions of emissions on each LOS. Magnetic field vectors \mathbf{B} were the fitting parameters of the emission regions, R_{in} and R_{out} . It was assumed that in each region there were cold and warm hydrogen atomic components. A hot component emitting at the

inner and/or outer region, which was unable to resolve by the Zeeman profile, gave broad Gaussian profiles beneath each spectra. These atomic temperatures of cold, warm and hot atomic components and spectral intensities were also used as fitting parameters.

Examples of the least-squares fit of the observed spectra with the above assumptions are shown in Fig. 2 with solid curves. The fitted results accord well with the exper-

Table 4 (continued) Fitted results from LOS 1 to 8 for the plasma of $R_{ax} = 3.80$ m.

LOS		inner		outer	
		cold	warm	cold	warm
LOS 5	hot				
R (m)	...		3.05		4.77
B (T)	...		2.41		1.49
θ (deg)	...		-26.6		42.7
ϕ (deg)	...		-11.9		4.96
Emission intensity (10^{18} ph s $^{-1}$ m $^{-2}$ sr $^{-1}$)	0.370		0.475		0.617
T_a (eV)	156	(0.183)	(0.292)	(0.168)	(0.449)
v_{LOS} (10^3 m/s)	11.9		4.49		-2.33
Relative proportion (%)	25.3	12.5	20.0	11.5	30.6
LOS 6					
R (m)	...		3.17		4.74
B (T)	...		2.79		1.54
θ (deg)	...		-20.2		42.3
ϕ (deg)	...		-13.4		2.12
Emission intensity (10^{18} ph s $^{-1}$ m $^{-2}$ sr $^{-1}$)	0.263		0.406		0.918
T_a (eV)	169	(0.173)	(0.232)	(0.314)	(0.604)
v_{LOS} (10^3 m/s)	22.4		4.88		-0.07
Relative proportion (%)	16.6	10.9	14.7	19.8	38.0
LOS 7					
R (m)	...		3.20		4.64
B (T)	...		3.07		1.72
θ (deg)	...		-20.3		39.2
ϕ (deg)	...		-17.3		-1.16
Emission intensity (10^{18} ph s $^{-1}$ m $^{-2}$ sr $^{-1}$)	0.257		0.203		0.837
T_a (eV)	170	(0.073)	(0.127)	(0.314)	(0.523)
v_{LOS} (10^3 m/s)	9.55		4.99		-0.20
Relative proportion (%)	19.8	5.9	9.8	24.2	40.4
LOS 8					
R (m)	...		3.88		4.78
B (T)	...		3.21		1.61
θ (deg)	...		6.88		55.3
ϕ (deg)	...		-8.42		1.65
Emission intensity (10^{18} ph s $^{-1}$ m $^{-2}$ sr $^{-1}$)	0.138		0.743		0.196
T_a (eV)	98.4	(0.343)	(0.400)	(0.093)	(0.103)
v_{LOS} (10^3 m/s)	27.2		-0.04		1.70
Relative proportion (%)	12.9	31.9	37.1	8.6	9.5

imentally observed spectra. Table 4 summarizes the fitted parameters from LOS 1 to LOS 8.

Temperatures of the cold atom components are ≤ 0.76 eV, while temperatures of the warm atom components range primarily from 1 eV to 15 eV. Temperatures of the hot atom components, produced by the charge exchange, range from 40 eV to 170 eV. When we compared the intensity contribution of the cold temperature components to that of the warm temperature components, we

found that, overall, the warm components are dominant or comparable to the cold components. Except for LOS 1 and 8, the inner and outer components move either toward the observer or from the periphery to the core plasma with a velocity of 2.4 km/s \sim 5 km/s and 0.07 km/s \sim 2.3 km/s, respectively, along the LOS.

A spatial extent of the emission region could make the σ^\pm components broader than the π components. The present H α profiles are complicated; however, we did not

clearly observe the broadening of the σ^\pm components. A variation of magnetic field strength of 0.05 T makes noticeable change on the spectral profiles. This limited the extent of the emission region and the uncertainty of the fitted emission locations, R_{in} and R_{out} which corresponded to a difference of $\leq \pm 0.05$ m.

Figure 1 (c) shows the fitting results for $R_{\text{ax}} = 3.80$ m. Emission intensity is plotted on the poloidal cross section from the fitted results. The area of the red circle is proportional to the sum of the intensity of emissions from both the cold and warm components.

It is unobvious whether this polarization separation technique is applicable for the upper or lower poloidal cross section, since the difference in the emission locations is expected to be closer. In addition there is a possibility that the emission locations are three points. Table 4 shows that one of the emission locations on LOS 8 is fitted at $R = 4.78$ m, where it seems like there is neither SOL nor divertor plasma around (Fig. 1 (c)). There is the emission contribution to the spectral profiles from the inner ($R \sim 3.6$ m), the outer ($R \sim 3.9$ m) and the outer divertor leg ($R \sim 5.2$ m). It is unable to distinguish among these three locations from the fitting. This LOS 8 fitting shows the limitation of the polarization separation observation technique. The outer divertor leg is close to the divertor plate.

For the temperatures of the cold and warm atomic components, T_a , the fitting numerical uncertainty was on a relatively low order of 0.01 eV. However, we assumed that the warm component was attributed to atoms dissociated from hydrogen molecules ($e + \text{H}_2 \rightarrow e + 2\text{H}(1s)$, 3 eV), those from hydrogen molecule ions ($e + \text{H}_2^+ \rightarrow e + \text{H}^+ + \text{H}(1s)$, 4.3 eV), those due to dissociative excitation of hydrogen molecules ($e + \text{H}_2 \rightarrow e + \text{H}(1s) + \text{H}(n = 3)$, 7.0 eV), or those from hydrogen molecule ions: ($e + \text{H}_2^+ \rightarrow e + \text{H}^+ + \text{H}(n = 2, 3)$, 1.5 eV). If this is the case, the profile should be different from the simple Gaussian shape assumed in the present fitting.

It is suggested that the hot component ranging from 39 eV to 170 eV is due to the charge exchange recombination and wall reflection [5, 6]. The inward velocities for hydrogen atoms are parameter sensitive to the peak position of π components. The fitting numerical uncertainty is as low as 0.01 km s^{-1} . However, here, we assumed that the cold and warm components had the same inward velocity in order to converge the fitting procedure. If this is not the case, we should separate the velocity components for the cold and warm components, as carried out in Ref. [9], where we exclude fine structure splittings. There is a factor of 2.5 on v_{LOS} parameters for cold and warm components.

For the other magnetic axial confinements, the same fitting procedures with the observed spectra have been carried out, and the results are plotted in Fig. 1. When the null point is far from the wall, the emission is located in the ergodic layer and the inward velocity is high. As the null point is closer to the wall, the emission outside of the ergodic layer increases and the velocity in the outside

area is low. For an inward magnetic axis configuration in Fig. 1 (a) $R_{\text{ax}} = 3.60$ m, the emission region surrounds the last closed flux surface (LCFS) and is located close to a stochastic region. The high emission intensity region is located along the inner X-point region. As the confined magnetic axis increases, the emission intensity of the outer region increases. For the outward configuration in Fig. 1 (d) $R_{\text{ax}} = 3.90$ m and (e) $R_{\text{ax}} = 4.00$ m, the emission locations accord well along the inner divertor leg. The velocity components along the LOS are directed toward the central plasmas.

4. Summary

We have observed polarization separation H α emission from the LHD plasmas. Multi-chordal observation is carried out for the different magnetic axes $R_{\text{ax}} = 3.60$ m, 3.70 m, 3.80 m, 3.90 m, and 4.00 m, respectively. We are able to deduce quantitative information from multi-code observations of the polarization separation spectra, i.e., emission intensities, locations, atomic temperatures and the LOS components of the velocities, via the simultaneous least-square fitting procedure to the orthogonal polarization components observed on a single LOS. The reconstructed H α emission plots on the poloidal cross section well describe the intensity distribution in the peripheral plasmas.

Acknowledgments

The authors are grateful to the LHD experimental group for their support during the course of the experiment and also appreciate Super-SINET for providing a real-time remote experiment environment. This work is performed with the support and under the auspices of the National Institute for Fusion Science Collaboration Research Program: New Diagnostics for High Temperature Plasmas No. 13 (FY:H13-H15), L4-32 3001-007 (FY:H16), NIFS04KOAP010 (FY:H17 and H18), NIFS06KCHP007 (FY:H18) and NIFS07KLPP308 (FY:H19). This research is partially supported by Grant-in-Aid for Scientific Research (C), 15540470 and 21540508, from the Japan Society for the Promotion of Science. One of the authors (A. I.) wishes to thank Mr. Tod Tollefson for his careful reading of the manuscript.

- [1] K. Ikeda *et al.*, *Progress in the ITER Physics Basis Nucl. Fusion* **47** (2007).
- [2] P.C. Stangeby, *The Plasma Boundary of Magnetic Fusion Device* (IoP, Bristol and Philadelphia, 1999).
- [3] C.H. Skinner *et al.*, *J. Nucl. Mater.* **241-243**, 887 (1997).
- [4] C.H. Skinner *et al.*, *J. Nucl. Mater.* **241-243**, 214 (1997).
- [5] H. Kubo *et al.*, *Plasma Phys. Control. Fusion* **40**, 1115 (1998).
- [6] A. Kumagai *et al.*, *Plasma Phys. Control. Fusion* **42**, 529 (2000).
- [7] M. Goto and S. Morita, *Phys. Rev. E* **65**, 026401 (2002).
- [8] T. Fujimoto and A. Iwamae, eds *Plasma Polarization Spec-*

- trosopy* (Springer, Berlin Heidelberg, 2008).
- [9] A. Iwamae *et al.*, Phys. Plasmas **12**, 042501 (2005).
[10] M. Shoji *et al.*, J. Nucl. Mater. **363-365**, 827 (2007).
[11] A. Iiyoshi *et al.*, Nucl. Fusion **39**, 1245 (1999).
[12] T. Watanabe *et al.*, *How to Use the Numerical System LHD_LINES_OF_FORCE.EXE for the Visualization of Line of Force in the Large Helical Device*, NIFS-TECH-14 (2006). in Japanese
<http://www.nifs.ac.jp/report/nifstech.html>
- [13] D.W. Willmarth *et al.*, *Thorium-Argon Spectral Atlas*,
<http://www.noao.edu/kpno/specatlas/thar/thar.html>
- [14] A. Iwamae *et al.*, Plasma Fusion Res. **4**, 042 (2009).